Earth and Planetary Science Letters 506 (2019) 23–37

Contents lists available at ScienceDirect

Earth and Planetary Science Letters

www.elsevier.com/locate/epsl

# Transient crustal deformation from karst aquifers hydrology in the Apennines (Italy)

Francesca Silverii [a,*], Nicola D'Agostino [b], Adrian A. Borsa [a], Stefano Calcaterra [c], Piera Gambino [c], Roberta Giuliani [d], Maurizio Mattone [d]

[a] Scripps Institution of Oceanography, University of California San Diego, La Jolla, CA, USA
[b] Istituto Nazionale di Geofisica e Vulcanologia, Centro Nazionale Terremoti, Rome, Italy
[c] Istituto Superiore per la Protezione e la Ricerca Ambientale, Rome, Italy
[d] Dipartimento della Protezione Civile, Rome, Italy

ARTICLE INFO

*Article history:*
Received 1 September 2018
Received in revised form 3 October 2018
Accepted 15 October 2018
Available online xxxx
Editor: R. Bendick

*Keywords:*
transient signal
GPS
karst aquifers
non-tectonic deformation
Apennines

ABSTRACT

The increasing accuracy and spatiotemporal resolution of space geodetic techniques have positively impacted the study of shallow crustal deformation in response to the redistribution of water masses. Measurable deformations have been documented in areas where snow and water variability is large and persists over sufficiently long periods. Here we analyze GPS time series and hydrological data from the Central-Southern Apennines, a tectonically-active region hosting large karst aquifers. We document the occurrence of regional-scale horizontal and vertical transient deformation that is clearly correlated to seasonal and multiyear hydrological variability. These transient signals, which are most strongly observed at GPS sites surrounding the main karst aquifers, modulate long term tectonic deformation. Our results suggest that the karst aquifers in this region experience alternating periods of expansion and contraction in response to increasing/decreasing precipitation and, consequently, higher/lower hydraulic head in the aquifers. Thanks to the availability of a dense continuous GPS network and complementary hydrological datasets, we are able to verify the processes causing the observed deformation. We model the shallow crust in the region as a continuous anelastic solid and use Green's functions for finite strain cuboid sources to estimate the strain rate distribution associated with the GPS observations. We use the $M_w$ 6.1 L'Aquila earthquake, which struck the Central Apennines in 2009 and whose effects are evident in geodetic data, to document the potential effects of moderate earthquakes on karst aquifers and to demonstrate the importance of correctly discerning tectonic from nontectonic signals in geodetic time series. Enhanced understanding of the karst aquifers behavior is of primary interest for improved management of this vital water resource and for a better understanding of the possible interactions between groundwater content and pore pressure variations in the crust and seismicity.



## 1. Introduction

Space geodetic techniques such as GNSS and InSAR, which provide temporally continuous and wide scale observations, are increasingly being used to detect transient signals of non-tectonic, hydrological origin at various spatial (tens of meters to hundreds of kilometers) and temporal (hours to years) scales and to estimate global and regional scale water mass redistribution and aquifer-system response (Argus et al., 2017). Rising awareness of the potential of hydrological forcing to significantly deform Earth's crust is furthermore drawing interest to possible interactions with tectonic stress and seismicity (Johnson et al., 2017) and on the correct estimation, detectability and possible misinterpretation of long-term trends and tectonic transients (Amoruso et al., 2017).

Since the elastic Earth response to surface loading acts primarily in the vertical direction, most investigations focus on the vertical component of the deformation. The horizontal component is however important because it can be used to better constrain the spatial distribution of loading (Wahr et al., 2013) and to highlight different kinds (e.g., anelastic) of responses to hydrological forcing, such as in alluvial or karst aquifers (King et al., 2007; Serpelloni et al., 2018).

In this paper, we analyze long (~12 yr) GPS time series spanning North-Central to Southern peninsular Italy, highlighting a hydrologically-related multiyear transient signal that is primarily expressed in the horizontal displacement components of GPS sites

* Corresponding author.
*E-mail address:* fsilverii@ucsd.edu (F. Silverii).

https://doi.org/10.1016/j.epsl.2018.10.019
0012-821X/

close to the carbonate aquifers. This work expands and substantiates our earlier study on a section of the Southern Apennines (Silverii et al., 2016), showing that similar hydrological processes pervasively affect karst aquifers along the entire Apennines mountain range with noticeable differences and complexities.

The Central-Southern Apennines represent a tectonically-active area, characterized by long-term ∼3mm/yr tectonic extension perpendicular to the mountain range (D'Agostino, 2014) and notably affected by moderate seismicity (Rovida et al., 2015). Two important seismic sequences recently struck this area: the L'Aquila sequence, which commenced with the mainshock on April 6, 2009 (Cheloni et al., 2014), and the Amatice-Norcia sequence, which began on August 24, 2016 and is still ongoing (Cheloni et al., 2017). We avoid the effects of the most recent sequence by analyzing displacement data only through August 23, 2016. Conversely, the $M_w$ 6.1 L'Aquila earthquake and its coseismic and postseismic effects are included in this study, offering a unique context for the analysis of the superimposition and possible interactions between hydrological and tectonic deformation.

We first present GPS and hydrological time series and describe the observed deformation. Given the large (hundreds of kilometers) spatial scales involved, we use a continuum approach to characterize the average poroelastic deformation of the shallow crust by applying the Green's functions for distributed strain sources by Barbot et al. (2017). Finally, we discuss the effects of tectonic and non-tectonic contributions in geodetic time series spanning the L'Aquila earthquake.

### 1.1. The carbonate aquifers of the Apennines

The Apennines range hosts extensive regional aquifers (blue shaded area in Fig. 1) consisting of Mesozoic carbonate rocks that are highly permeable due to the karst and fissuring processes resulting from their recent tectonic history (Boni, 2000). The Quaternary evolution of the Apennines was characterized by crustal extension and regional uplift, which caused extensive block faulting, dropping of base levels, and, locally, the deposition of thick continental depositional sequences between carbonate ridges. The latter, altering the base flow level and affecting groundwater flow of the surrounding fractured carbonate aquifers, hinders the development of a mature karst network in the discharge areas. Consequently, water circulation at lower elevations takes place mainly through a dense net of fractures, and groundwater flow does not immediately respond to seasonal recharge from precipitation (Romano et al., 2013). At their contact with the carbonate aquifer, the deposits act as a permeability boundary giving rise to the basal springs of the regional groundwater, with mean discharges between 1 and 18 $m^3/s$ (Boni et al., 1986; Boni, 2000). In many cases, the heterogeneity of these deposits (clastic fluvial, lacustrine, and travertine deposits all with different permeabilities, Petitta et al., 2015) leads groundwater seepages from carbonate aquifers, favoring the recharge of alluvial aquifers by karst aquifers (Schurch and Vuataz, 2000). In summary, the carbonate massifs of South-Central Italy have mature karst features in higher-elevation recharge areas, but rarely in discharge areas (Amoruso et al., 2013).

## 2. Data

### 2.1. GPS data

We use daily observations from 186 permanent GPS stations in Central and Southern Italy, most of which belong to the Rete Integrata Nazionale GPS network (RING; Avallone et al., 2010). We select GPS time series with at least 4.5 yr of data between epochs 2004.5000 (July 1, 2004) and 2016.6434 (August 23, 2016), and we exclude stations possibly affected by ongoing volcanic deformation along the Tyrrhenian coast. To reduce the common mode signal, we adopt an updated version of the Eurasian terrestrial reference frame described in Métois et al. (2015). In order to emphasize the long-term, secular ∼3mm/yr NE–SW directed active extension across the Apennines, we reference GPS station velocities to a frame defined by minimizing the horizontal velocities of stations located on the Tyrrhenian coast (Fig. 1). Details about GPS data processing are described in Section S1 of Supplementary materials, and the coordinates and velocities of analyzed stations are listed in Supplementary Table S2.

We attempted to remove effects of long-wavelength (hundreds of kilometers) hydrological and atmospheric loading from the GPS times series (full details in Section S2 of Supplementary Materials). This correction, however, caused a noticeable increase (up to 70%) in time series variance, especially for the horizontal components. Since the transformation to the Eurasian reference frame, which lowers the common mode error at a continental scale, is likely to partially remove the effects of large scale loads, we decided not to explicitly correct the GPS time series.

The GPS time series (Figs. 2 and S6) show noticeable annual and multiyear oscillations superimposed on the long-term (∼2004.5–2016.6) tectonic trend. The horizontal components of these oscillations exhibit symmetry about an axis running roughly along the crest of the Apennines from Northern to Southern Italy (hereafter, "central axis"), with stations on either side moving systematically towards and away from each other. This effect is particularly strong at sites near carbonate rocks along the Apennines and decreases towards the Tyrrhenian and Adriatic coasts.

We quantify the behavior of multiyear oscillations in terms of deviations in time series slope relative to its long-term trend. From the time of local maxima and minima shared by several horizontal time series, we highlight five episodes of opposite inward (T1: 2006.4–2008.8, T3: 2011.5–2012.75, T5: 2014.0–2016.6) and outward (T2: 2008.8–2011.5, T4: 2012.75–2014.0) motion (Fig. 2). Starting from the detrended time series, we estimate the slopes and associated uncertainties of the longest (≥2.25 yr) time intervals T1, T2 and T5, only considering GPS stations having at least 60% of the possible observations in each interval (Fig. S7). Hereafter, if not specified differently, we refer to the velocity deviations in the different time intervals simply as "velocity".

The spatial pattern of the calculated horizontal velocities clearly shows alternate shortening/extensional episodes across the central axis of the Apennines, with consistent behavior from Central to Southern Apennines (Fig. 3, top). In particular, stations with the largest velocities (up to 5 ± 0.8 mm/yr) are preferentially located close to the limestone massifs hosting large karst aquifers, whereas more distant sites are characterized by lower velocities (≤1.5 mm/yr) and do not display a clear evidence of such multiyear deformation. Note that we do not include GPS sites in the near-field (∼30 km radius) of the L'Aquila earthquake in the T2 analysis (Fig. 3, central panel) to avoid introducing potential bias from transient deformation associated with the event.

The GPS vertical component has a lower signal-to-noise ratio than the horizontal components, which could obscure patterns of vertical multiyear signals at individual stations. Clear multiyear oscillations are however visible in several vertical time series of Central Apennines (e.g., sites highlighted in yellow in Fig. 2) and show, in accordance with the horizontal components, alternate trends (up to ∼7 ± 2 mm/yr) in the selected time intervals. We find two main patterns of vertical velocities: one associated with sites close to karst aquifers, and one with sites near or outside them (Fig. 3 bottom). To enhance the signal-to-noise ratio, we stack the daily values of detrended vertical time series for several selected stations with long records and clear multiyear trends (Fig. 4). We cluster stations in three groups: (a) sites on karst aquifers of Cen-

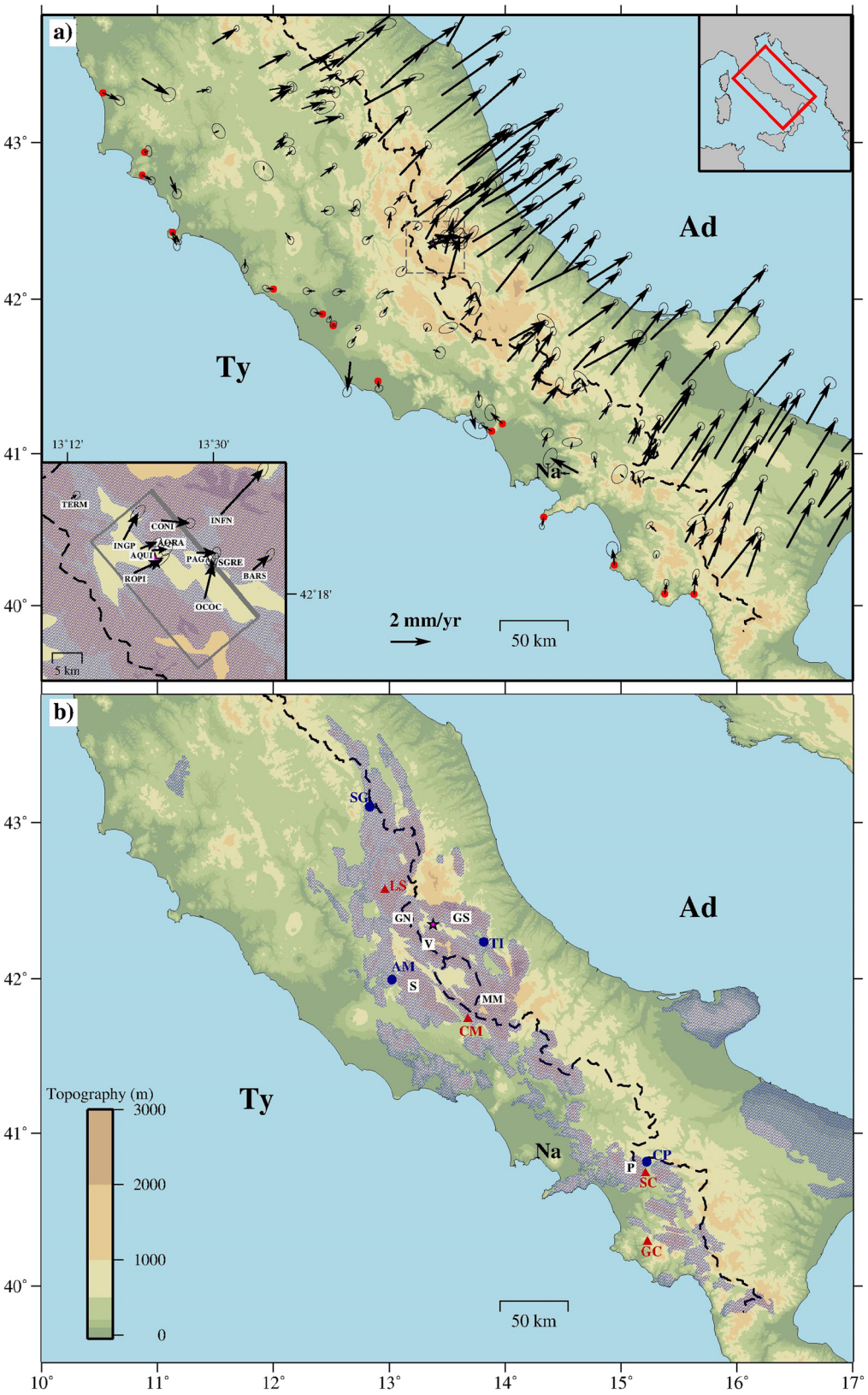


**Fig. 1.** Map of the study area (red rectangle in the top right inset). a) GPS horizontal long-term velocities in a Tyrrhenian reference frame with 95% CI ellipses (black arrows). Red circles indicate the GPS sites used to define this reference frame. The black dashed line sketches the drainage divide and the magenta star indicates the position of L'Aquila 2009 mainshock epicenter. The bottom left inset shows a zoom over L'Aquila area (dashed rectangle in the map), where the gray rectangle is the surface projection of the fault plane model from Cheloni et al. (2014) and the blue areas outline the exposures of carbonate rocks as shown in b). b) Hydrological data source locations. The blue areas outline the exposures of carbonate rocks. The blue circles and red triangles respectively indicate the location of San Giovenale (SG), Acqua Marcia (AM), Tirino (TI) and Caposele (CP) springs and Leonessa (LS), Campoli Appennino (CM), Senerchia (SC) and Gioi Cilento (GC) rain gauges. The initials with white background indicate the location of the main hydrological units mentioned in the main text: Giano-Nuria (GN), Velino (V), Gran Sasso (GS), Simbruini (S), Monti della Meta (MM) and Picentini (P). (For interpretation of the colors in the figure(s), the reader is referred to the web version of this article.)

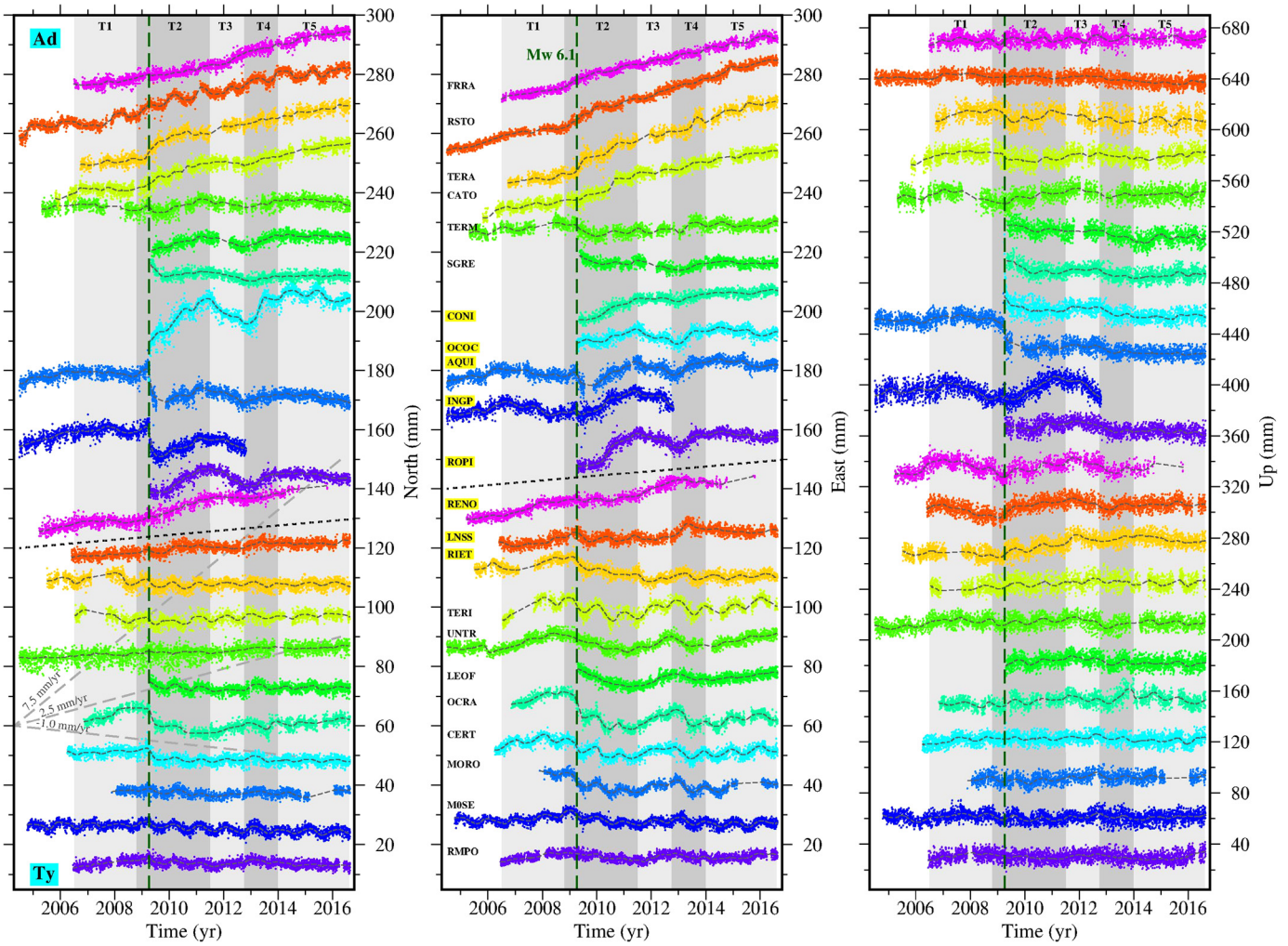


**Fig. 2.** Observed (colored dots) North (left), East (center) and Up (right) displacements time series for selected sites along a cross section across Central Apennines (see Fig. S5 for the stations locations). The black dashed lines represent a 6 month Gaussian filter of the time series (i.e., the weights are given by the Gaussian function, and the width is 6 times the conventional Gaussian sigma). GPS sites are ordered from the Tyrrhenian coast (Ty, bottom) toward the Adriatic coast (Ad, top). The vertical gray stripes outline 5 time intervals of alternating multiyear trends. The vertical dashed line indicates L'Aquila earthquake mainshock epoch (notice that the coseismic offset has been previously removed). The dotted black oblique lines separate stations characterized by symmetrical horizontal behavior. The station names highlighted in yellow denote sites with clear multiyear vertical trend.

tral Apennines, affected by multiyear signal on both horizontal and vertical components; (b) sites near karst aquifers, affected by multiyear signal on both horizontal and vertical components, but with different vertical motion to sites in group (a); and (c) sites far from karst aquifers without significant multiyear deformation on the horizontal components, but affected by vertical signal similar to group (b). The vertical stacked time series are roughly opposite and phase-shifted between the sites of group (a) and those of groups (b) and (c). These results show that sites near karst aquifers display a prevailing vertical signal (uplift) positively correlated with transient dilatation centered on karst aquifers. Sites farther from the karst aquifers and not significantly affected by horizontal show the opposite behavior, with prevailing negative vertical signal (subsidence) during phases of horizontal dilatation centered on karst aquifers.

### 2.2. Hydrological data

Climate in Central and Southern Apennines is of the mountain variety of the Mediterranean type, with rainy/snowy autumn-winters and dry summers. Similar to the rest of Southern Europe, precipitation patterns are influenced by global climate phenomena such as the North Atlantic Oscillation (De Vita et al., 2012; Romano and Preziosi, 2013). The temporal climatic patterns of the Apennines strongly control the recharge of karst aquifers, which occurs prevalently in winter and spring (due to direct precipitation and snow melt at high altitudes).

Here we present two kinds of observables providing information about hydrology of the region under examination: rainfall data at representative rain gauges, and discharge data at some of the main karst springs of the Apennines. The hydrological data sources are summarized in Supplementary Table S3.

#### 2.2.1. Rainfall data

Annual precipitation in our study area ranges from 1000 mm to 2000 mm (at the highest elevations), with rainfall typically reaching a maximum in November and a minimum in July (Di Matteo et al., 2013; Allocca et al., 2014). We show cumulative monthly rainfall data (Fig. 5) of four rain gauges that, for their record completeness and their position, can be assumed as indicative of the precipitation trend in the last decade in the Central (Leonessa and Campoli Appennino) and South-Central (Gioi Cilento and Senerchia) Apennines (Fig. 1). Detrended daily cumulative precipitation from Leonessa and Campoli Appennino is also shown in Fig. 4 to accentuate deviations relative to the long-term (∼2003–2016.8) average trend. The data show a similar pattern from Central to

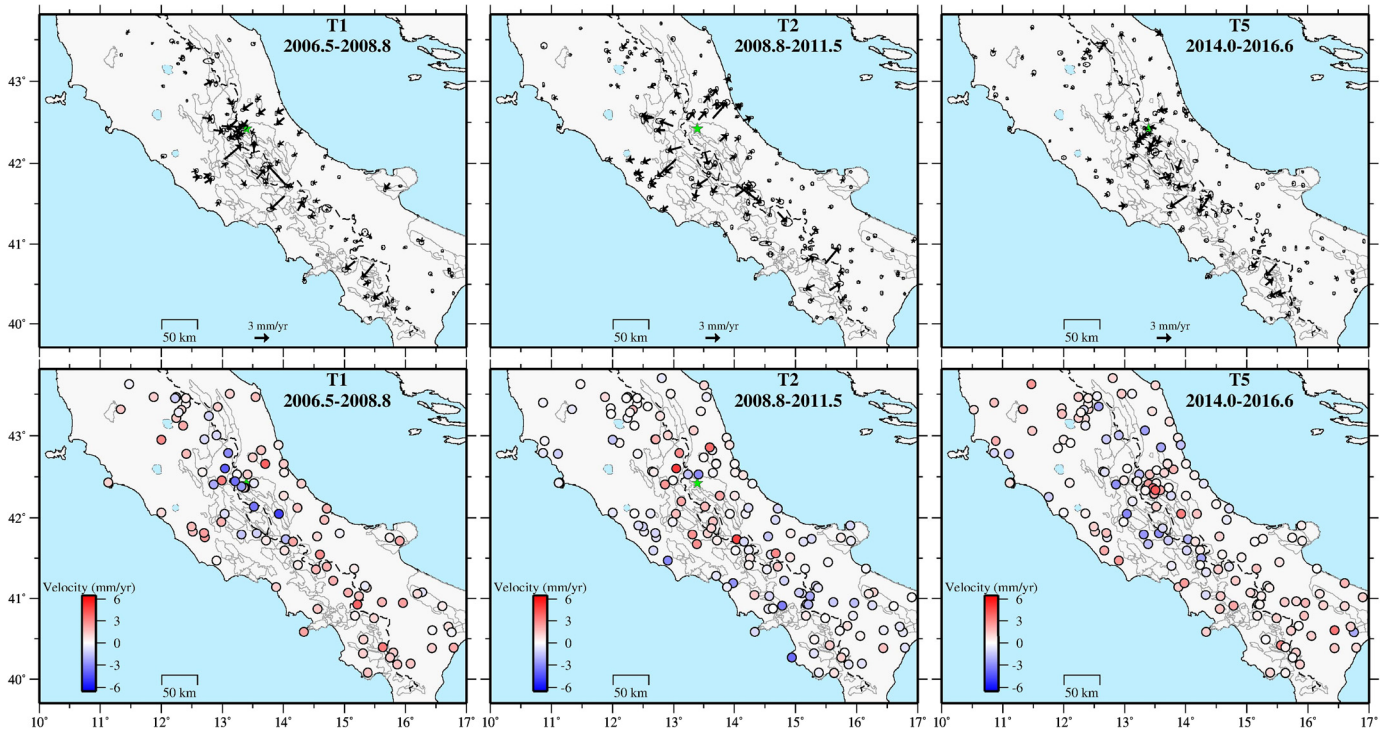


**Fig. 3.** Observed horizontal (top; black arrows with 95% CI ellipses) and vertical (bottom; color coded circles) GPS velocities calculated as deviation from the long-term trend in the three selected time intervals (T1, T2 and T5) corresponding to distinct multiyear hydrological trend variations. The gray lines contour the carbonate aquifers of the Apennines and the black dashed line sketches the drainage divide. The green star indicates the position of L'Aquila 2009 mainshock epicenter. Note that sites in the near field of L'Aquila epicenter have been excluded in the T2 interval.

Southern Apennines, with precipitation generally concentrated in November–February, but subject to noticeable multiyear variability such as the significant reduction during droughts in 2006–2008, 2012 and 2014–2016.8. The previously identified 5 time intervals clearly correspond to periods of anomalously low (T1, T3, T5) or high (T2, T4) precipitation.

*2.2.2. Spring discharge data*

We present discharge data (Fig. 5) for four karst springs along the Apennines (locations in Fig. 1). The San Giovenale spring, located in the northern part of the Central Apennines at 475 m a.s.l., has a mean discharge of 0.36 $m^3/s$. The Acqua Marcia springs, in the Central Apennines, are composed of several springs located between 322 and 329 m a.s.l. at the northern end of the Simbruini Mts. aquifer and have a mean discharge of about 5 $m^3/s$. The Tirino river springs are located at the south-eastern boundary of Gran Sasso massif and are fed by the main groundwater flow in this part of the aquifer (Amoruso et al., 2013; Fiorillo et al., 2015b). Discharge data refer to a gauging station (Bussi Madonnina, Abruzzo) along the Tirino river, where waters coming from the main springs are collected. Being direct runoff from the Tirino catchment negligible, the river flow mainly corresponds to spring discharge from the higher part of the Tirino valley (Amoruso et al., 2013; Fiorillo et al., 2015b). The mean discharge calculated at the Bussi gauging station is about 6 $m^3/s$. The data show only small seasonal changes, but noticeable variations over longer (∼4 yr) periods (Boni et al., 2002). The Caposele spring is one of the largest karst springs of Southern Italy (417 m a.s.l., mean discharge 4 $m^3/s$). Located along the north-eastern boundary of the Picentini Mountains, it is primarily fed by the Cervialto massif (Celico and Civita, 1976) and can be considered the only basal spring draining this aquifer (Fiorillo et al., 2015a). The time series of this spring have already made an important contribution to the understanding of hydrologically-related deformation for Southern Apennines (Silverii et al., 2016).

Despite differences in local characteristics of the aquifers feeding these springs (e.g. geological–geomorphological setting, karst conditions, areal extent of catchment), some clear common features stand out between the discharge time series (Fiorillo et al., 2015a). In particular, the seasonal maximum discharge usually occurs in springtime, some (∼4–5) months after the precipitation peak (Fig. 5). The smooth shape and delayed discharge present in all the hydrographs indicate that the spring discharge is in general not affected by single rainfall events, but respond to the precipitation accumulated over several months (Fiorillo and Doglioni, 2010). This is mainly due to the prevalence of diffuse flow through fractures (Section 1.1) and can be influenced by further factors such as the time shift between snowfall and snow melt, the extent of the catchment area, and the potential presence of low-permeability barriers to subsurface water flow. Furthermore, all the hydrographs show clear multiyear fluctuations in response to successive years of decreasing/increasing precipitation. In particular, the 5 time intervals defined on the basis of GPS data match with multiyear aquifer depletion (T1, T3, T5) or recharge (T2, T4) periods (Fig. 5). In agreement with previous results obtained in a limited part of the Apennines, the close correlation between geodetic transient signals and hydrological phases of recharge/discharge of karst aquifers, points to a causal relationship between deformation and hydrological factors.

## 3. Comparison between GPS and hydrological time series

As previously highlighted, both the geodetic and hydrological time series show alternating trends in successive multi-year intervals (Figs. 2 and 5). The GPS horizontal time series at stations close to the karst aquifers are highly correlated with spring discharge, as emphasized in Fig. 6, where we compare the East component at selected GPS sites and some hydrological time series. We perform cross-correlation analysis after applying a low-pass 6-months Gaussian filter to the time series (i.e., the weights are given by the

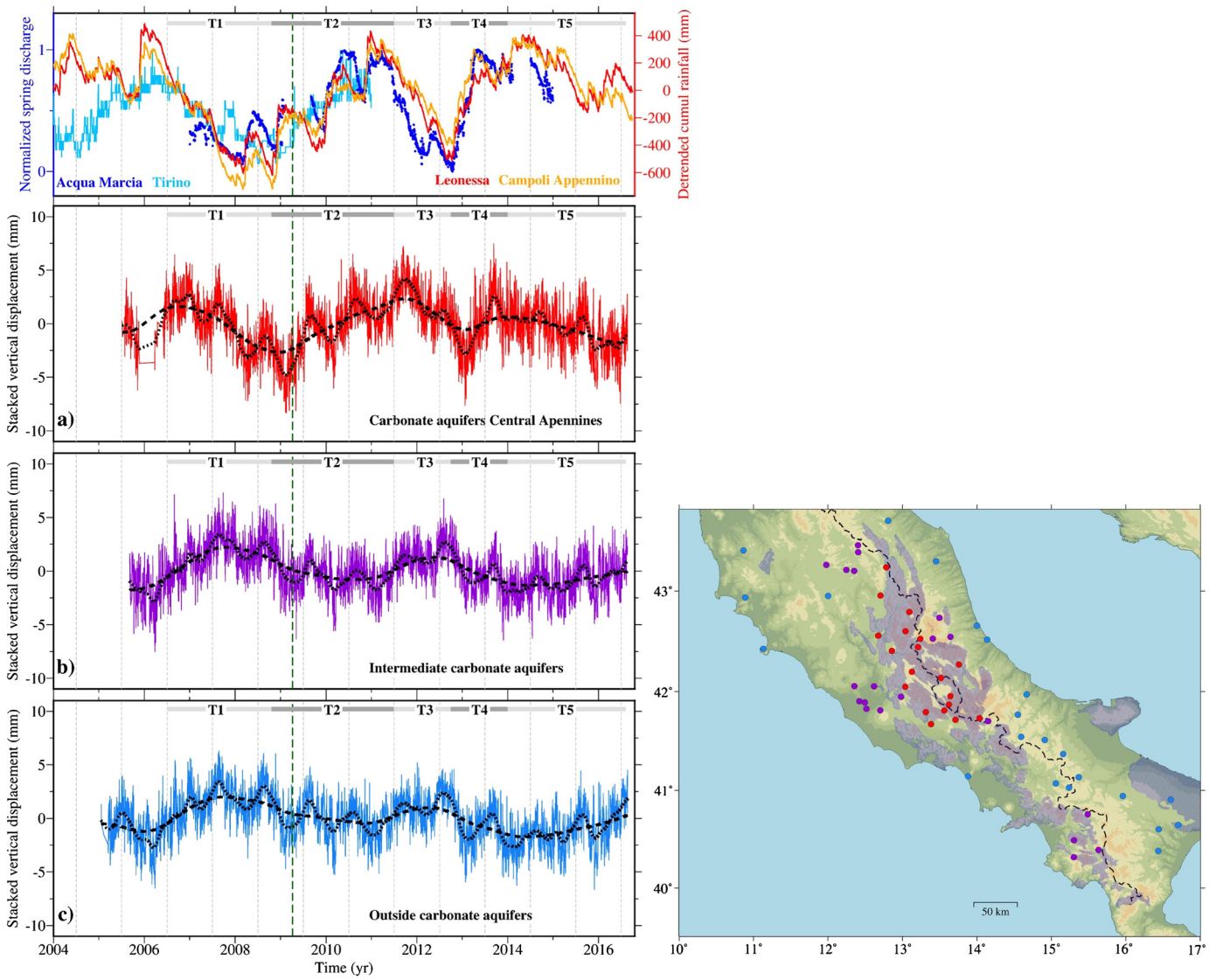


**Fig. 4.** Comparison between hydrological time series (spring discharge – blue lines, cumulative detrended rainfall – red and orange lines) and vertical daily time series (colored lines) obtained by stacking data from three groups of selected stations (highlighted with different colors). 6 months (black dotted line) and 2.5 yr (black dashed line) filtered (Gaussian filter) stacked time series are also displayed. The vertical dashed line indicates L'Aquila earthquake mainshock epoch. The map shows the location of the sites used to compute the stacked time series for the carbonate aquifers of a) Central Apennines group (red line in time series and related stations in map); b) intermediate carbonate aquifers (purple) and c) outside carbonate aquifers (blue). See table S4 for the list of stations used to calculate the stacked time series. Note that the sites in the very near field of L'Aquila mainshock epicenter have not been included in the time series stacking.

Gaussian function, and the width is 6 times the conventional Gaussian sigma). The results show high correlation values with minimal (±0–1 month) time delay between deformation and discharge (negative/positive delay corresponds to deformation preceding/following spring discharge) (Fig. 7). This is the case not only at the local (<10 km) scale, e.g., between Acqua Marcia springs and CERT station (correlation 0.81, 13 days delay, distance = 9 km) and Caposele spring and MCRV station (0.94, −22 days, 6 km), but also at larger scales, e.g., between Acqua Marcia spring and CERA (0.88, −19 days, 90 km) and MCRV (0.82, −5 days, 220 km). These observations confirm the regional nature of the presented hydrological records, i.e., the hydrological records can be used as a proxy for karst water storage both near and far from the point of observation (the variability in the time delays is probably due to local hydrogeological features). In the reasonable assumption of a linear relationship between spring discharge and water table elevation in the aquifers, these observations also suggest that the observed horizontal deformation depends, to first order, on processes sensitive to the hydraulic head inside karst aquifers.

Hydrological deformation in the Southern Apennines (Silverii et al., 2016) and Eastern Alps (Serpelloni et al., 2018) is characterized by significant anisotropy between the horizontal and vertical components, assumed to be due to different physical forcing mechanisms. Horizontal deformation in these regions has been associated with variable hydrostatic pressure in the fractured karst aquifers, whereas the more spatially uniform vertical signal has been related to the elastic response to hydrological loads acting at continental scales (Silverii et al., 2016; Serpelloni et al., 2018). This elastic load response, causing subsidence in high precipitation periods and uplift in drought periods, is visible in most of the vertical time series analyzed in our work, including those from sites located far from the Apennines and showing no noticeable horizontal deformation (Fig. 4c) and many located on or near karst aquifers (Fig. 4b). However, several sites we analyzed in the Northern and Central Apennines (e.g. ALRA, INGP, LNSS, RENO, RIET and TERM in Figs. 2, S6 and S7) respond roughly isotropically to hydrological forcing (Fig. 4a). These sites show positive correlation (∼0.7) with spring discharge in both verti-

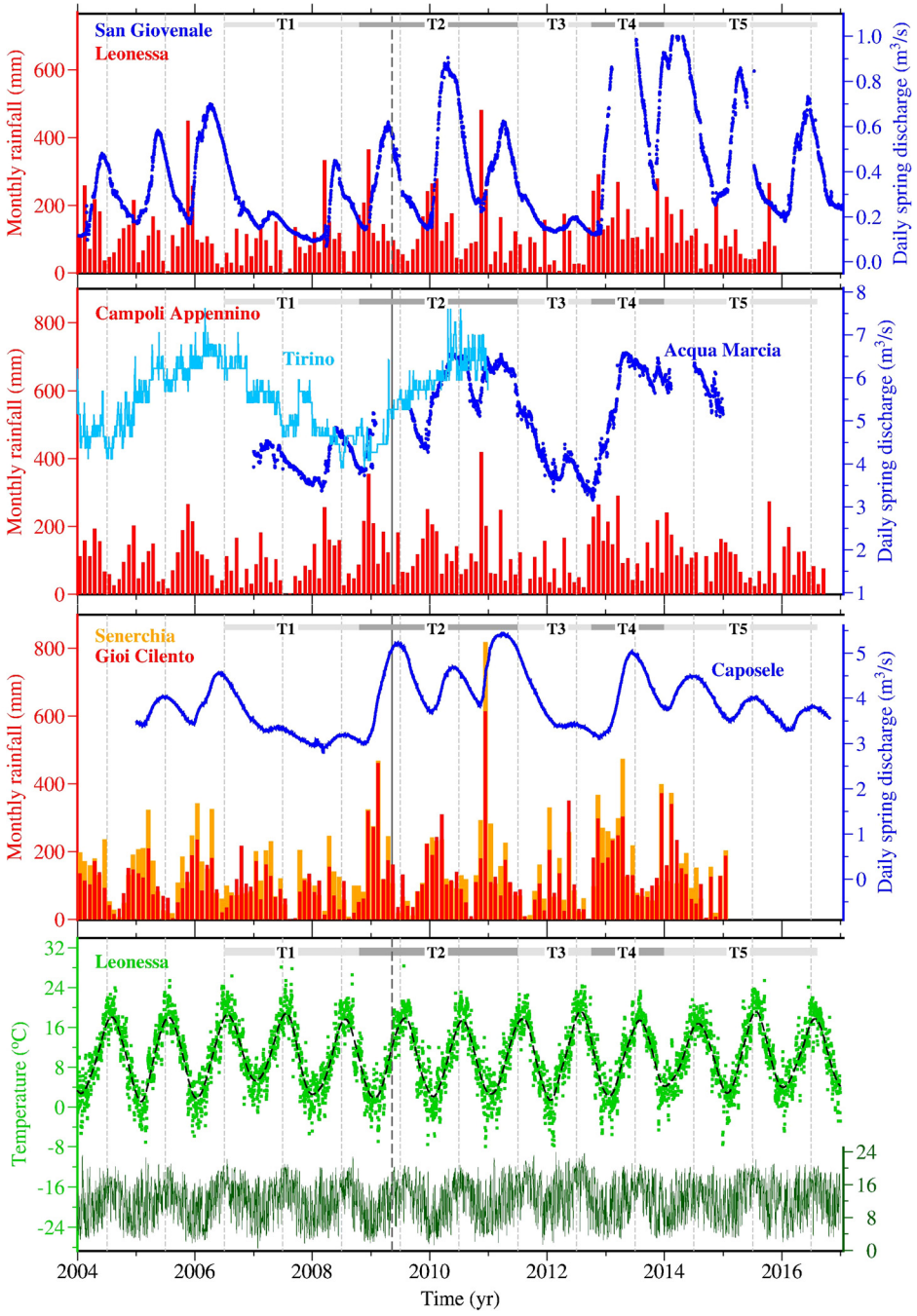


**Fig. 5.** Hydrological time series from Northern, Central and Southern Apennines. From top to bottom: 1) cumulated monthly rainfall records at Leonessa (red) rain gauge and daily discharge data of San Giovenale spring (blue curve); 2) cumulated monthly rainfall records at Campoli Appennino (red) rain gauge and daily discharge data of Tirino (light-blue curve) and Acqua Marcia (blue curve) springs; 3) cumulated monthly rainfall records at Gioi Cilento (red) and Senerchia (orange) rain gauges and daily discharge data of Caposele spring (blue curve). The bottom plot shows the temperature records at Leonessa site: mean (green squares) records and its 6-months filter (black dashed line) and the difference between maximum and minimum temperatures (dark green). The location of rain gauges, thermometric station and springs are indicated in Fig. 1. The vertical line indicates L'Aquila earthquake mainshock epoch.

cal and horizontal components, implying that periods of aquifer recharge are associated with vertical uplift and horizontal extension. This behavior is particularly prominent at the multiyear scale and cannot be simply related to the poroelastic response of alluvial aquifers, since not all the sites showing this behavior are located on alluvial aquifers and, vice versa, not all the sites on alluvial aquifers show this kind of response. The subsiding trend associated with the severe 2006–2008 drought (interval T1) and the subsequent uplift associated with the sequence of high precipitation years between 2009 and 2011 (interval T2) are notably distinctive (Fig. 4a).

In the Central Apennines, the spatial distribution of interannual velocity changes (Fig. 3) shows an approximately radial pattern around the main carbonate aquifers, roughly following the spatial distribution of the carbonate massifs. This pattern suggests that most of the deformation is associated with the large hydrogeological units from GN-V and MM (Fig. 1), whereas the GS massif seems to play a less important role. A smaller but consistent horizontal deformation pattern also characterizes some sites in Central Italy located near but not right over the carbonate aquifers in the vicinity of the L'Aquila earthquake (e.g., M0SE, MORO and TERA in Figs. 2 and 3). As discussed later (Sections 4.2.1 and S3), the veloc-

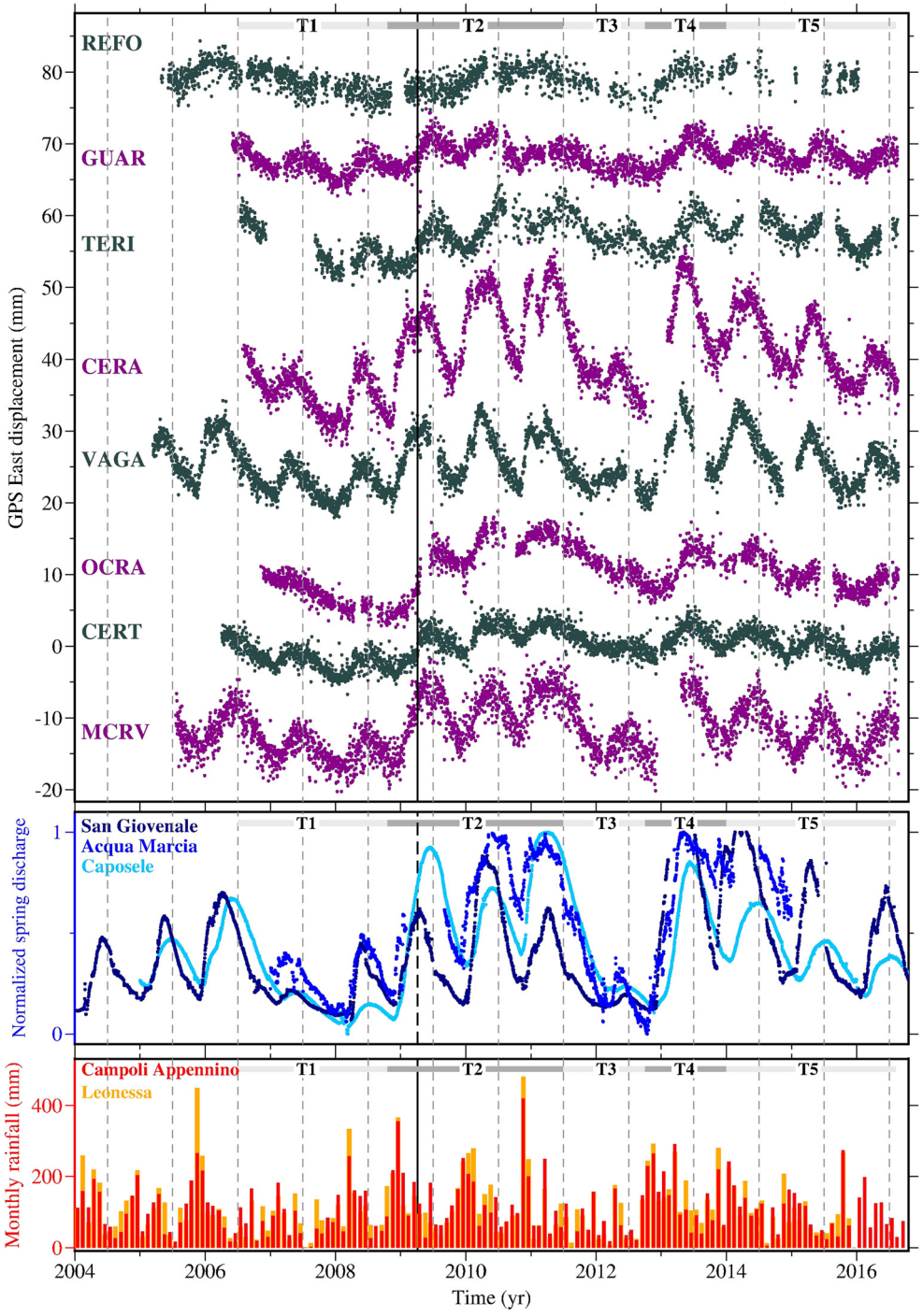


**Fig. 6.** Comparison between selected GPS time series (East component) and hydrological records (monthly rainfall and normalized springs discharge). Note that displacements for CERT, GUAR, OCRA, TERI and VAGA are inverted for clarity. The vertical line indicates L'Aquila earthquake mainshock epoch.

ity estimations at these sites could be partially (<20–30%) affected by the effect of postseismic processes of the 2009 L'Aquila event.

In summary, a general deformation pattern can be recognized: during periods of high precipitation and consequent sustained aquifers recharge (e.g. intervals T2 and T4), the sites on/near the carbonate aquifers experience horizontal extension and vertical uplift; whereas an opposite trend characterizes low precipitation periods (e.g., intervals T1, T3 and T5). The sites outside karst aquifers experience lower/negligible horizontal deformation and roughly opposite multiannual vertical behavior relative to sites on the aquifers. This vertical behavior is likely related to the elastic Earth response to surface loads acting at large (continental/regional) scales, with subsidence during high precipitation periods and uplift in dry periods (Figs. 3 and 4). We expect that the elastic response to surface loading affects the vertical deformation of the entire region under examination, but it is partially/entirely obscured by the various (poroelastic) processes occurring in the karst regions.

## 4. Discussion

The results presented in the previous sections show a clear correlation between the transient deformation at GPS sites and the hydrological time series representing the trends of recharge and

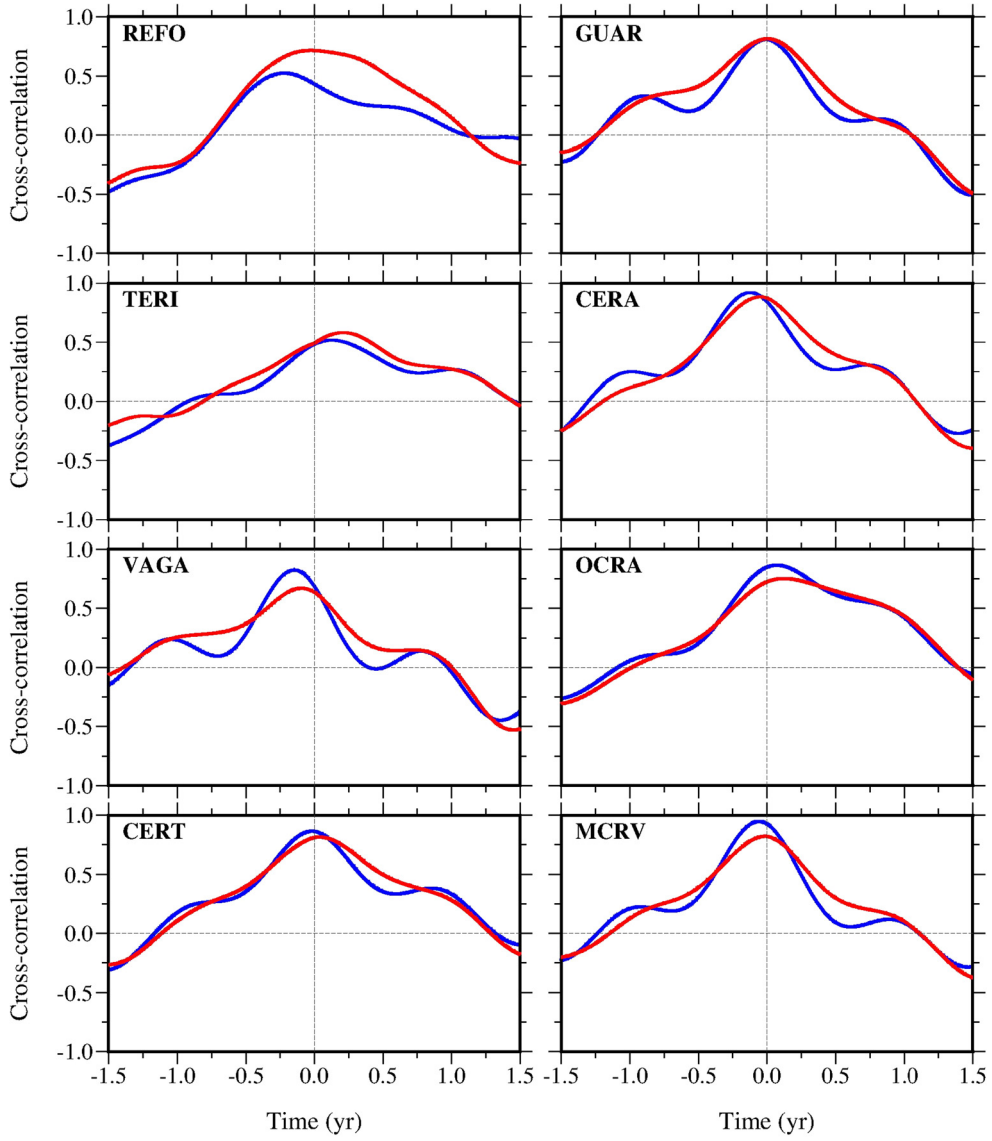


**Fig. 7.** Cross correlation analysis between the GPS (East component) shown in Fig. 6 and Acqua Marcia (red line) and Caposele (blue line) 6-months filtered (Gaussian filter) time series. Note that vertical axis for CERT, GUAR, OCRA, TERI and VAGA is inverted for clarity.

discharge of the main carbonate aquifers of the Apennines. The pattern and magnitude of observed horizontal deformation are not likely related to the elastic response of the solid Earth to surface loading that, conversely, would cause subsidence and smaller (by a factor of 2–3, Wahr et al., 2013) horizontal inward motion toward the loads during periods of high hydrological loading.

Due to the presence of topographic relief, we considered the possible contribution of the thermoelastic strain due to surface temperature variations (Ben-Zion and Leary, 1986; Tsai, 2011). The temperature data at Leonessa (Fig. 5) show seasonal peak-to-peak variations of up to ∼35 °C and show that drought periods (e.g. 2006–2008 and 2012) are characterized by higher temperatures and slightly lower (∼4 °C) peak-to-peak amplitudes relative to those in wet periods (e.g., 2009–2011). As estimated by Silverii et al. (2016) in a similar context, the deformation associated with such temperature variations cannot explain the amplitude of the multiyear signal observed in the horizontal time series, but could contribute slightly (∼1–3 mm) to the observed vertical displacements, especially at seasonal periods.

Since neither elastic response to surface loading nor thermoelastic strain can explain observed GPS deformation, we consider an alternative explanation based on volumetric anelastic strain due to changes in karst aquifer hydraulic head.

### *4.1. Distributed anelastic strain rate from karst aquifers filling and draining*

#### *4.1.1. Model*

According to simplified water circulation models in unconfined karst aquifers (Fiorillo, 2011; Amoruso et al., 2013), the spring discharge fluctuations can be associated with variations in the aquifer hydraulic head $\Delta h$, which would result in internal pressure variations given by $\Delta P = \rho_w g \Delta h$ ($\rho_w$ water density, $g$ gravitational acceleration). Carbonate aquifers can experience considerable seasonal fluctuations in the height of the water table, up to several tens of meters (LeGrand and Stringfield, 1971; Bella et al., 1998; Milanović, 2014). The spatial distribution of observed surface deformation (near/on the main aquifers of the Apennines) and its correlation with spring discharge suggest that deformation is related to the variation of the hydraulic head inside the aquifers in the shallow crust and, in particular, to the opening

of conductive, interconnected water-filled fractures that pervade the carbonate aquifers of the Apennines (Section 1.1).

GPS data highlight a deformation pattern with nearly isotropic episodes of expansion/contraction in most of Central Apennines and mostly anisotropic horizontal deformation with a preferential NE–SW expansion direction in South-Central Apennines. The origin of this effect is unclear but is possibly related to the cumulated result of several fractures and microcracks within the fractured karst system and to their preferential alignment. An accurate simulation of this process would require specific information (fractures spacing, dimension, aperture, and penetration depth) about the spatial distribution and mechanical characteristics of the karst aquifers that is not available at the broad scale of our analysis area. We instead apply a continuum approach to the aquifer domain, using the Barbot et al. (2017) Green's functions for distributed deformation to infer an upper crust strain rate distribution consistent with the hydrological trend deviations. Barbot et al. (2017) calculated closed-form solutions for the displacement and stress generated by an arbitrary distribution of anelastic deformation in the Earth's interior, where the deformation was assumed to be related to thermodynamically irreversible processes (e.g. thermoelasticity, poroelasticity, and viscoelasticity). The solution, given for anelastic deformation in finite cuboid volumes embedded in a uniform elastic half space, can be linearly combined to form more complex configurations of strain.

We separately invert the hydrologically related GPS velocities in time intervals T1, T2 and T5 to estimate the corresponding distribution of strain rates ($\dot{e}_{11}, \dot{e}_{22}, \dot{e}_{33}$; axis $x_1$ and $x_2$ oriented respectively perpendicularly and in parallel to the Apennines axis, $x_3$ vertical axis) within a three-dimensional grid of 8 km × 8 km × 1 km cuboids over our analysis area (Fig. 8). We assume typical continental crust values for Poisson's ratio (0.25) and shear modulus (30 GPa). We use regularized least squares inversion to solve the direct problem

$$\begin{bmatrix} \vec{d} \\ \mathbf{0} \\ \mathbf{0} \end{bmatrix} = \begin{bmatrix} \boldsymbol{G} \\ k\nabla^2 \\ \gamma \boldsymbol{C_p} \end{bmatrix} \vec{m},$$

where $\vec{d}$ is a $1 \times 3N_s$ vector of North/East/Up velocity observations ($N_s$ = number of sites) and $\vec{m}$ is the $1 \times (3N_c + 3)$ model vector of strain rates ($N_c$ = number of cuboids). The matrix $\boldsymbol{G}$ includes the Green's functions related to the 3 strain rate components, and an additional 3 columns (one for each component North, East, Up) that assimilate rigid translation rates common to the whole dataset (e.g. related to common mode noise and smoothly-varying atmospheric and hydrological signals with wavelength comparable to the model area which affect similarly all GPS sites). We weight the observations by multiplying $\vec{d}$ and $\boldsymbol{G}$ by a diagonal weight matrix $\boldsymbol{W}$ formed by the inverse of velocity uncertainties (no covariance components are included). $\nabla^2$ is a 3-d finite-difference approximation of the Laplacian operator, and the factor $k$ controls the amount of smoothing and is selected from a trade-off curve between model roughness and data misfit. $\boldsymbol{C_p}$ is a matrix composed of zeroes and ones used to penalize strain in cuboid sources outside surface exposure of carbonate rocks. The weight of this penalization is controlled by the hyperparameter $\gamma$ that has been selected by performing trial inversions and choosing the value that provides negligible strain rate outside the carbonate areas. We tested the inversion sensitivity by varying the number of cuboid layers (i.e. the model depth) and determined the best fit model associated to every model depth value.

#### 4.1.2. Results

Fig. 8 shows the dilation rate and calculated velocities for the three selected time intervals from our best-fit strain rate solutions for a model depth of 5 km. Our strain rate models successfully reproduce the main pattern of observed surface deformation in the T1 (Fig. 8, top), T2 (middle) and T5 (bottom) time intervals, including the vertical deformation in the proximity of karst aquifers. These results strongly suggest that poroelastic aquifer deformation, induced by variations in hydraulic head and elastically coupled to the surrounding crust, provides a realistic, first-order description of GPS-observed surface deformation. The generally smaller-amplitude deformation outside the aquifers is mostly due to the elastic Earth response to anelastic aquifer deformation and, especially for the vertical component, likely reflects common-mode translation due to large scale processes.

The distribution of dilatation rate shown in Fig. 8 highlights the different contributions of various hydrostructures, as the main role played by the aquifers between GN-V and MM in the Central Apennines and the lower influence of minor aquifer units and of the GS aquifer (particularly visible in the T5 interval thanks to increased availability of nearby GPS stations). This pattern could reflect the high infiltration capacity (Boni, 2000) and the high homogeneity of hydrogeological behavior of the large hydrogeological units extending from the GN-V to MM and, conversely, the stratigraphic irregularity characterizing the extreme northeast sector of the Abruzzi Apennines (e.g., GS massif), at the margin of the carbonate shelf, where the regional thrust fault act as a primary aquitard (Boni, 1975).

From the standpoint of interpreting our models in terms of changes in hydraulic head (or aquifer water storage), one challenge is that source depth and the magnitude of dilatation rate are not uniquely constrained by the inversion, since the same level of data fit can be achieved with different values of model depth and because the dilatation rate inducing a specific level of surface deformation increases with increasing model depth. We can partly resolve this problem by focusing on relative, rather than absolute, changes. For this analysis, we compute the total model dilatation rate $\sum_1^{N_c}(\dot{e}_{11+}\dot{e}_{22} + \dot{e}_{33})$ and the mean dilatation rate for each of the 3 time periods (T1, T2, T5), and the ratio of both between T1/T2 and between T1/T5 (Table 1). Comparing results for models at both 5 km and 2 km depth, we note that the ratios are independent of model depth and are thus robust features of our analysis.

If we assume that positive/negative dilatation rates are associated with increasing/decreasing water table height changes inside the aquifers, then the calculated dilatation ratios indicate the relative rate of water volume change in different hydrological phases. For comparison, we calculate the same ratios from rainfall rate and spring discharge time series (Table 1). We only include time series with sufficient (60%) data in the three time intervals, and we omit results for San Giovenale springs, which are not compatible with the other data due to their dominant seasonal fluctuations and a slightly anticipated response (i.e., discharge occurs earlier than corresponding changes in the other springs). The resulting ratios are compatible with those from the strain rate models. Specifically, the average T1/T2 ratios are 0.98 (strain rate), 1.14 (rainfall), 1.13 (discharge), which are within 16% of each other. The T1/T2 ratios are uniformly lower than the corresponding T1/T5 ratios of 1.82, 2.51 and 2.03 (respectively), which exhibit more scatter. This analysis, while not comprehensive, provides an independent confirmation of the model results and suggests a direction for further model validation.

In a complementary study, D'Agostino et al. (submitted for publication) applied this model to analyze the correlation between hydrologically induced deformation and seismicity in a spatially constrained area in Southern Apennines, where a dense seismic network is available.

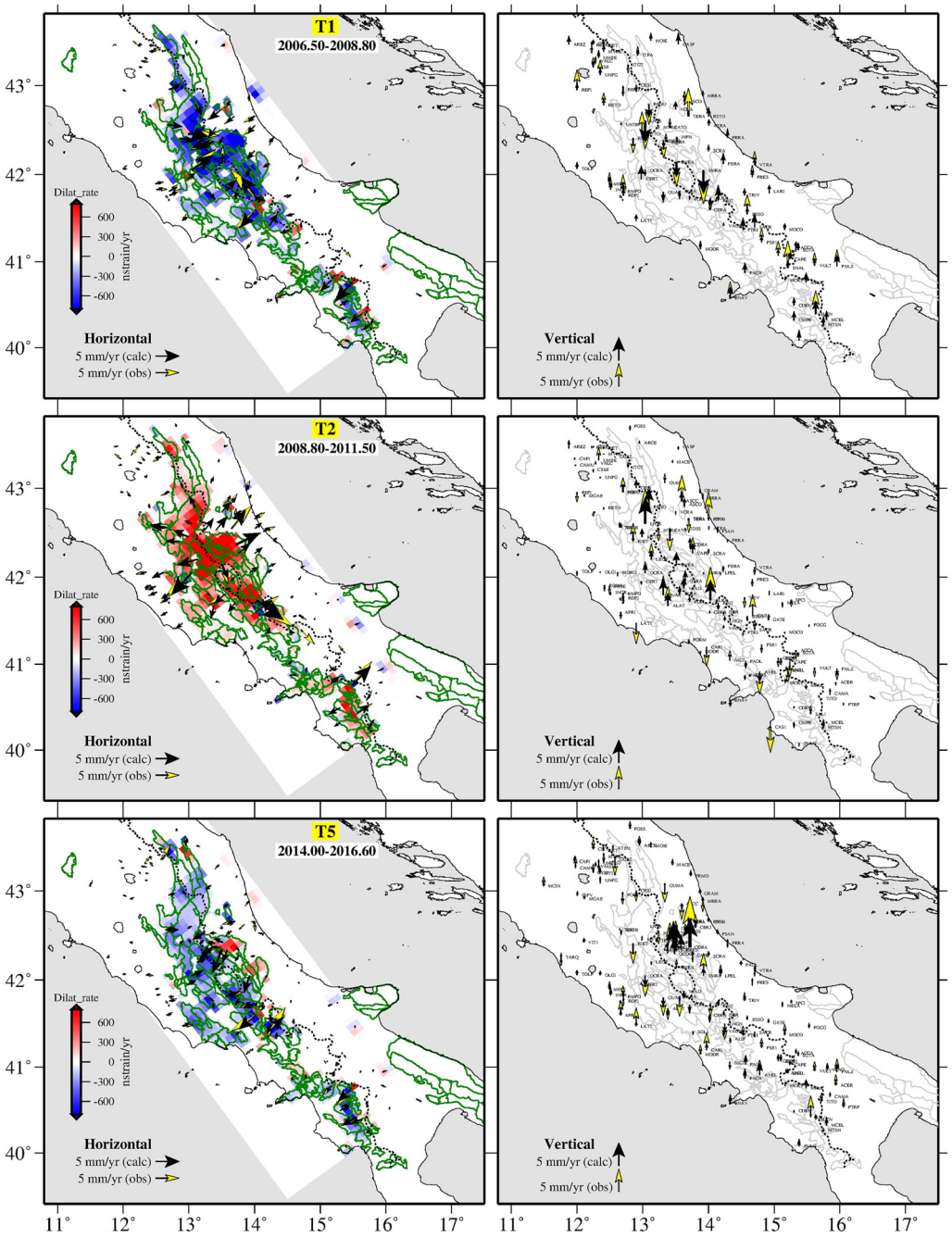


**Fig. 8.** Examples of best fit model results for T1 (top), T2 (center) and T5 (bottom) intervals. The left panels show the cuboids grid, the dilatation rate values (color coded) calculated for each cuboid and the observed (yellow arrows) and modeled (black arrows) horizontal velocities. The green contours outline the main carbonate aquifers. The right panels show the observed (yellow arrows) and modeled (black arrows) vertical velocities; the carbonate aquifers contours are represented as gray lines.

### *4.2. The L'Aquila earthquake*

The 2009, $M_W$ 6.1 L'Aquila earthquake occurred after a strong 2006–2008 drought period (interval T1) and at the beginning of a multiyear high precipitation period (interval T2) (Fig. 5). Since this event was located in the Central Apennines (inset in Fig. 1), nearby GPS sites were influenced by both the hydrologically induced deformation described above and the coseismic and postseismic displacements associated with the earthquake (Cheloni et al., 2014). In the following paragraphs, we discuss the possible consequences of the spatial proximity of this seismic event to big karst aquifers. In particular, we examine the influence of earthquake-related deformation on the estimation of hydrologically induced deformation and the effect of the latter on the identification and interpretation of transient signals possibly related to the earthquake.

#### *4.2.1. Surface displacements from the L'Aquila earthquake*

The L'Aquila mainshock occurred on a ~50°SW dipping, 135°–140°N striking normal fault (inset in Fig. 1; Cheloni et al., 2014) located ~15 km east of the drainage divide that separates regions of opposite horizontal motion due to hydrology (i.e. the "Tyrrhenian" and "Adriatic" sides, Figs. 2 and 3).

GPS and InSAR observations over an area extending ~30 km from the epicenter recorded visible postseismic deformation, mainly related to afterslip, with an exponential time-decay constant of $\tau$ ~10–30 days (i.e. ~99% of the postseismic signal occurred in the first ~100 days after the mainshock) (Cheloni

**Table 1**
Comparison between the rates calculated in the three time intervals T1, T2 and T5 from the total and mean dilatation rates and several hydrological time series. The T1, T2 and T5 columns report, for each interval, the mean dilatation rates estimated by the inversion using two different model depths and the slopes estimated from spring discharge and cumulative detrended rainfall time series. The last two columns display the ratios of T1 and, respectively, T2 (yellow background) and T5 (green) rates and show a good agreement between the ratio values calculated from the different sources.

| Quantity \ Time interval | | T1 | T2 | T5 | T1/T2 | T1/T5 |
|---|---|---|---|---|---|---|
| **Total dilatation rate (nstrain/yr)** | Depth 2 km | -254148.57 | 266299.12 | -136555.14 | 0.95 | 1.86 |
| | Depth 5 km | -422588.40 | 420109.98 | -237825.17 | 1.01 | 1.78 |
| **Mean dilatation rate (nstrain/yr)** | Depth 2 km | -83.33 | 87.31 | -44.70 | 0.95 | 1.86 |
| | Depth 5 km | -55.42 | 55.10 | -31.19 | 1.01 | 1.78 |
| **Cumulative rainfall rate (mm/yr)** | Leonessa | -283.42 | 229.88 | -102.84 | 1.23 | 2.75 |
| | Campoli Appennino | -312.35 | 290.22 | -138.09 | 1.07 | 2.26 |
| | Senerchia | -390.71 | 328.84 | X | 1.18 | X |
| | Gioi Cilento | -384.03 | 355.57 | X | 1.08 | X |
| **Spring discharge rate ($(m^3/s)/yr$)** | Tirino | -0.90 | 0.93 | X | 0.98 | X |
| | Caposele | -0.57 | 0.45 | -0.28 | 1.27 | 2.03 |

et al., 2014; Gualandi et al., 2014). In general, the observed postseismic displacement shows a NE orientation on the north-eastern side of the fault (foot-wall block, e.g. CATO and TERA in Fig. 2), a SW orientation on the south-western side of the fault (hanging-wall block, e.g. AQUI, INGP and ROPI in Fig. 2) and subsidence at the sites on the hanging-wall block in the near field of the fault (e.g., AQUI, CONI, INGP, OCOC, ROPI and SGRE in Fig. 2).

At longer time spans (∼years) and larger spatial wavelength (tens of km), postseismic viscoelastic relaxation could potentially affect the motion of GPS sites in Central Italy, with an amplitude and spatial pattern dependent on the thickness of the elastic upper crust and the viscosity of the lower crust/upper mantle. Generally, if the viscoelastic source is fairly deep, coseismic and postseismic horizontal displacements have the same sign, whereas their vertical displacements have opposite signs (Feigl and Thatcher, 2006). As shown by simple postseismic viscoelastic models of L'Aquila earthquake (Silverii, 2016, Section 6.3.1), the horizontal viscoelastic deformation associated with L'Aquila earthquake would be directed to the NE on the foot-wall block and to the SW on the hanging-wall block, whereas the direction of vertical deformation (uplift) would be opposite to that produced by coseismic slip and afterslip, over an area dependent on the elastic layer thickness (Feigl and Thatcher, 2006).

The L'Aquila horizontal postseismic deformation (related to both afterslip and viscoelastic relaxation) would therefore generate diverging displacement across the fault, with a direction similar to that of the hydrological deformation in the same period (interval T2). The exception is the motion of the hanging-wall block of the fault on the right side of the drainage divide, where the hydrological trend and the postseismic deformation have opposite directions, as shown by the time series of AQUI, CONI and INGP in Figs. 2 and 9. This postseismic deformation could potentially influence the estimation of the long-term trend and, consequentially, the trend deviations in time intervals T1, T2 and T5, particularly at sites located adjacent to the SW and NE sides of the faults. The earthquake moderate magnitude and the remarkable similarity between the detrended time series of sites in the epicentral area with those of Southern and North-Central Apennines (Fig. 9) rule out a substantial variation of the velocity estimation, even if we can't exclude some effect (up to ∼20–30%), especially in the T2 interval (a detailed analysis is reported in Section S3 of Supplementary Material).

#### *4.2.2. Evidence for a transient aquifer response to the L'Aquila earthquake*

The broad similarity of hydrologically-induced deformation across Southern and Central Italy (Section 3) provides an opportunity to use the displacement time series of sites likely not affected by the L'Aquila earthquake as a baseline for identifying deformation anomalies in the near-field of the seismic event. In Fig. 9 we compare time series of several stations in the epicentral hanging-wall region of the fault (AQUI, INGP, ROPI and TERM) with two distant stations not significantly affected by the earthquake: MRLC, located ∼250 km south in the Southern Apennines, and RENO, located ∼50 km north of the epicenter, used as a proxy for the peculiar vertical deformation of the aquifers of Central Apennines.

As shown in GPS velocity maps (Fig. 3) and vertical stacked GPS time series (Fig. 4), the drought period preceding the L'Aquila earthquake (interval T1) generated horizontal contraction and subsidence across the large aquifers of Central Apennines. The L'Aquila

earthquake, which occurred at the beginning of interval T2, modified the subsequent displacement behavior of nearby stations in the hanging wall of the fault. The nominal motion of these stations from ongoing hydrological deformation should have been to the north and east in the horizontal (Fig. 9a–b, station MRLC) and uplifting in the vertical (Fig. 9c, station RENO). Instead, the coseismic offset and the afterslip-related deformation caused a clear anomaly in the North (rapid, decaying southward motion), East (westward motion) and Up (subsidence) displacements over several months following the earthquake.

Approximately 8 months after the mainshock, hydrological deformation took over from afterslip as the dominant source of surface deformation. Interestingly, at some sites this recovery occurred at higher rates than expected without the earthquake occurrence (e.g., horizontal components at AQUI, INGP and ROPI in Fig. 9a–b). At INGP the expected uplift related to the high precipitation period T2 underwent a rate increase starting from 2009.9 (Fig. 9c), consistent with InSAR-observed acceleration in the same area (Moro et al., 2017).

A mechanism for these rate anomalies is suggested by observations that in aquifers dominated by fracture porosity and permeability, seismic shaking can change aquifer properties due to the formation of micro-cracks (Casini et al., 2006), unblocking of pre-existing fractures, fracture cleaning, and/or fracture dilatancy and closing (Brodsky et al., 2003; Wang and Manga, 2010). Several works have highlighted clear post-earthquake effects on fractured aquifers in the Central-Southern Apennines (Celico, 1981; Carro et al., 2005). Both short-term (minutes to hours) and medium-term (weeks to months) effects following L'Aquila earthquake have been recorded in several kinds of hydrological observations (Amoruso et al., 2011; Adinolfi Falcone et al., 2012). In particular, Amoruso et al. (2011) associate the observed medium-term effects to transient changes in permeability induced by fracture cleaning and unblocking of pre-existing fractures, with the most significant impact close to the coseismic rupture area and reaching maximum values about 3 years after the event. We suggest that the rate increase observed in the GPS time series is related to temporary changes in groundwater hydrodynamics (i.e. increase of hydraulic conductivity parameter) that accelerate the ongoing deformation related to aquifer recharge in T2.

#### *4.2.3. Hydrological deformation preceding L'Aquila earthquake*

Previous studies, using InSAR data, reported subsidence starting three years (∼2006) before the L'Aquila mainshock in the nearby Pizzoli and Preturo plains (a minor discharge area of the GN-V hydrostructure; Moro et al., 2017) and in a wider region located ∼20–30 km SW of the mainshock fault (Atzori et al., 2013). This subsidence was interpreted to be a preseismic phase of the mainshock (Moro et al., 2017) or was suggested to be related to the fluid pressure variability within the crust occurring contemporaneously with, and possibly in advance of, large earthquakes (Atzori et al., 2013).

Given the spatially distribution of the highlighted preseismic subsidence (corresponding to the GN-V hydrostructure and its secondary discharge areas), its timing (coinciding with the aquifer depletion period T1), the analogous behavior (i.e. vertical subsidence in drought periods – T1, T3 and T5 – and uplift in periods of high precipitation – T2 and T4) observed at GPS sites tens of kilometers far from L'Aquila area (e.g. ALRA, LNSS, RENO and RIET in Figs. 2, S6 and S7), and the general presence of alternate multiyear periods of uplift and subsidence, we propose an alternative interpretation that associates the observed subsidence preceding L'Aquila earthquake to non-tectonic multiyear hydrological deformation acting at the scale of the entire Central Apennines.

Recently Devoti et al. (2018), focusing on a local area around L'Aquila, drew similar conclusions about the presence of hydrologically-driven multiyear deformation and the non-tectonic cause of the preseismic subsidence. We show that this deformation affects all Apennines and we insert the vertical displacement observed at INGP in a larger context involving the main aquifers of Central Apennines.

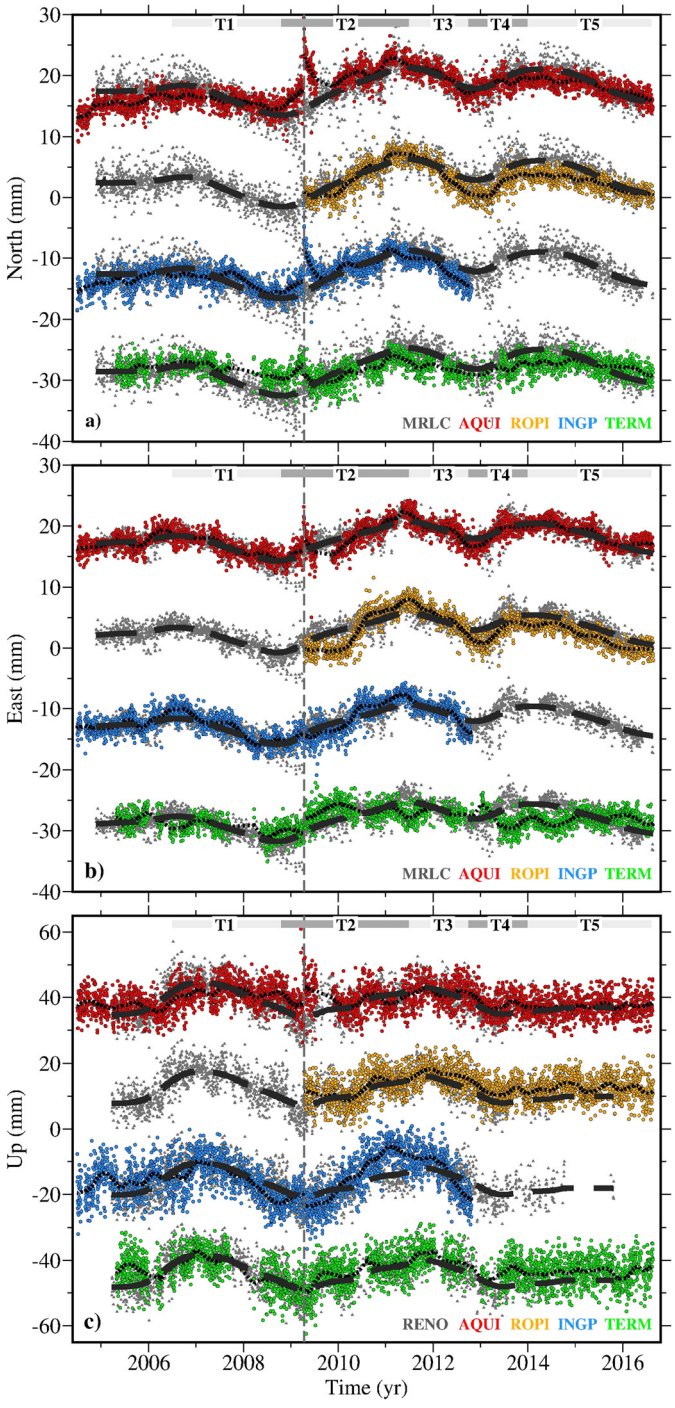


**Fig. 9.** Comparison between the time series of some selected sites in the very near field of L'Aquila mainshock epicenter, AQUI, INGP, ROPI and TERM (colored circles and superimposed 6-months Gaussian filter – dotted lines) and time series at MRLC (for North and East components) and RENO (for the Up component), that are used as a reference for comparison (black triangles in the background and thick black dashed lines in the foreground representing a 2.5 yr Gaussian filter). In case of time series with both pre- and post-mainshock data, the post-mainshock data have been vertically shifted in order to superimpose with the reference time series and make the trend comparison more clearly visible. The vertical axis for the East component of TERM site has been reversed for sake of comparison.

## 5. Conclusions

By integrating GPS with hydrological data, we highlight a noticeable non-tectonic transient signal over a broad region from Central to Southern Apennines. This finding underlines the potential of certain hydrogeological environments, such as karst aquifers, to produce significant deformation at large scales that can be recorded by geodetic instruments. The significance is twofold: i) spatial geodetic data such as those from dense GNSS networks are revealing unexpected usefulness in the study of aquifer properties at accuracies and spatiotemporal resolutions not achievable with traditional hydrological datasets; ii) considerable non-tectonic deformation can overlap and modulate both long-term and transient tectonic signals.

Regarding the first point, we highlight the similar response (expansion in high precipitation periods and contraction in drought periods) of the main aquifers of the Apennines to common hydrological forcing. However, we also see significant differences between aquifers, as the nearly isotropic deformation of the main aquifers of Central Italy compared to the more anisotropic response of Southern Apennines, or variability in the deformation response of different hydrological units, which likely reflects the different recharge conditions and storage capacity of different aquifers and the depth reached by the deformation process. We apply the solutions for distributed anelastic strain by Barbot et al. (2017) to model non-tectonic deformation. This model inevitably represents an oversimplification of the relevant physics, but it provides a useful continuum approach to characterize the average anelastic deformation of the shallow crust at large spatial scales and it suggests that the karst aquifers of the Apennines are indeed the source of much of the observed crustal deformation in Southern and Central Italy.

The Apennines, analogous to other mountainous regions of the world such as the Himalayas, are deforming because of both tectonic (e.g., interseismic and co- and post-seismic) and non-tectonic (e.g., hydrologically-induced) processes. The occurrence of L'Aquila earthquake in the time span under examination clearly stresses the importance of taking into account significant non-tectonic signals in the estimation and identification of long-term velocities and small amplitude tectonic deformation. As we pointed out in the GPS times series of the L'Aquila epicentral area, the co-location of large aquifer systems and active faults likely favors post-earthquake effects on fractured aquifers, as has been observed also during the recent Central Italy sequence (Petitta et al., 2018).

## Acknowledgements

We are grateful to the editor Rebecca Bendick and two anonymous reviewers for their careful reviews and insights. We would like to thank Marianne Métois, James D.P. Moore and Sylvain Barbot for helpful discussions. We thank Gerardo Ventafridda, Acquedotto Pugliese S.p.A., for providing Caposele spring discharge data. This work was funded in part by the National Science Foundation, grant number EAR-1614218.

The RINEX daily files from RING GPS stations can be accessed at http://ring.gm.ingv.it, while the other GPS data can be obtained by contacting the author N. D'Agostino (nicola.dagostino@ingv.it).

Leonessa and Campoli Appennino rain gauges are managed by Ufficio Idrografico of Regione Lazio (http://www.idrografico.roma.it). Gioi Cilento and Senerchia rain gauges are managed by Protezione Civile Regione Campania (http://centrofunzionale.regione.campania.it/index.php/rete-di-monitoraggio; data updated until December 2014).

San Giovenale springs data are recorded by Arpa Umbria (http://www.arpa.umbria.it). Tirino springs data are available upon request from Servizio Idrografico e Mareografico Regione Abruzzo (http://www. regione.abruzzo.it/xIdrografico/). Acqua Marcia springs discharge data have been provided by ACEA S.p.a. The discharge data of Caposele spring have been provided by The Aqueduct Company of Puglia (Acquedotto Pugliese S.p.A.).

Figures have been produced by using Generic Mapping Tools (GMT) software (Wessel et al., 2013).

## Appendix A. Supplementary material

Supplementary material related to this article can be found online at https://doi.org/10.1016/j.epsl.2018.10.019.

## References

Adinolfi Falcone, R., et al., 2012. Changes on groundwater flow and hydrochemistry of the Gran Sasso carbonate aquifer after 2009 L'Aquila earthquake. Ital. J. Geosci. 131 (3), 459–474. https://doi.org/10.3301/IJG.2011.34.

Allocca, V., Manna, F., De Vita, P., 2014. Estimating annual groundwater recharge coefficient for karst aquifers of the southern Apennines (Italy). Hydrol. Earth Syst. Sci. 18, 803–817. https://doi.org/10.5194/hess-18-803-2014.

Amoruso, A., Crescentini, L., Petitta, M., Rusi, S., Tallini, M., 2011. Impact of the 6 April 2009 L'Aquila earthquake on groundwater flow in the Gran Sasso carbonate aquifer, Central Italy. Hydrol. Process. 25, 1754–1764. https://doi.org/10.1002/hyp.7933.

Amoruso, A., Crescentini, L., Petitta, M., Tallini, M., 2013. Parsimonious recharge/discharge modeling in carbonate fractured aquifers: the groundwater flow in the Gran Sasso aquifer (Central Italy). J. Hydrol. 476, 136–146. https://doi.org/10.1016/j.jhydrol.2012.10.026.

Amoruso, A., Crescentini, L., Chiaraluce, L., 2017. Surface temperature and precipitation affecting GPS signals before the 2009 L'Aquila earthquake (Central Italy). Geophys. J. Int. 210 (2), 911–918. https://doi.org/10.1093/gji/ggx210.

Argus, D.F., et al., 2017. Sustained water loss in California's mountain ranges during severe drought from 2012 to 2015 inferred from GPS. J. Geophys. Res., Solid Earth 122 (12), 10559–10585. https://doi.org/10.1002/2017JB014424.

Atzori, S., Chiarabba, C., Devoti, R., Bonano, M., Lanari, R., 2013. Anomalous far-field geodetic signature related to the 2009 L'Aquila (central Italy) earthquake. Terra Nova 25, 343–351. https://doi.org/10.1111/ter.12040.

Avallone, A., et al., 2010. The RING network: improvement of a GPS velocity field in the central Mediterranean. Ann. Geophys. 53 (2), 39–54. https://doi.org/10.4401/ag-4549.

Barbot, S., Moore, J.D.P., Lambert, V., 2017. Displacement and stress associated with distributed anelastic deformation in a half-space. Bull. Seismol. Soc. Am. 107 (2), 821–855. https://doi.org/10.1785/0120160237.

Bella, F., Biagi, P.F., Caputo, M., Cozzi, E., Della Monica, G., Ermini, A., Plastino, W., Sgrigna, V., 1998. Aquifer-induced seismicity in the central Apennines (Italy). Pure Appl. Geophys. 153 (1), 179–194. https://doi.org/10.1007/s000240050191.

Ben-Zion, Y., Leary, P., 1986. Thermoelastic strain in a half space covered by unconsolidated material. Bull. Seismol. Soc. Am. 76, 1447–1460.

Boni, C.F., 1975. The relationship between the geology and hydrology of the Latium-Abruzzi Apennines. In: Parotto, M., Praturlon, A. (Eds.), Geological Summary of the Central Apennines. Quad. Ric. Sci. 90, 301–311. Structural Model of Italy.

Boni, C.F., 2000. Karst aquifers of the Central Apennines (Les aquifères karstiques de l'Apennines Central). Hydrogéologie 4, 49–62.

Boni, C.F., Bono, P., Capelli, G., 1986. Schema Idrogeologico dell'Italia Centrale – A) Carta idrogeologica (scala 1:500.000); B) Carta idrologica (scala 1:500.000); C) Carta dei bilanci idrogeologici e delle risorse idriche sotterranee (scala 1:1.000.000). Mem. Soc. Geol. Ital. 35 (2), 991–1012.

Boni, C., Pianelli, A., Pierdominici, S., Ruisi, M., 2002. Le grandi sorgenti del fiume Tirino (Abruzzo). Boll. Soc. Geol. Ital. 121, 411–431.

Brodsky, E.E., Roeloffs, E., Woodcock, D., Gall, I., Manga, M., 2003. A mechanism for sustained ground water pressure changes induced by distant earthquakes. J. Geophys. Res. 108. https://doi.org/10.1029/2002JB002321.

Carro, M., De Amicis, M., Luzi, L., 2005. Hydrogeological changes related to the Umbria–Marche earthquake of 26 September 1997 (Central Italy). Nat. Hazards 34, 315–339. https://doi.org/10.1007/s11069-004-2074-0.

Casini, S., Martino, S., Petitta, M., Prestininzi, A., 2006. A physical analogue model to analyse interactions between tensile stresses and dissolution in carbonate slopes. Hydrogeol. J. 14, 1387–1402. https://doi.org/10.1007/s10040-006-0064-x.

Celico, P., 1981. Relazioni tra idrodinamica sotterranea e terremoti in Irpinia (Campania). Rend. Soc. Geol. Ital. 4, 103–108.

Celico, P., Civita, M., 1976. Sulla tettonica del massiccio del Cervialto (Campania) e le implicazioni idrogeologiche ad essa connesse (On the tectonics of the Cervialto Massif (Campania) and related hydrogeological issues). Boll. Soc. Nat. Napoli 85, 555–580.

Cheloni, D., et al., 2014. Coseismic and post-seismic slip of the 2009 L'Aquila (central Italy) $M_w$ 6.3 earthquake and implications for seismic potential along the

Campotosto fault from joint inversion of high-precision levelling, InSAR and GPS data. Tectonophysics 622, 168–185. https://doi.org/10.1016/j.tecto.2014.03.009.

Cheloni, D., et al., 2017. Geodetic model of the 2016 Central Italy earthquake sequence inferred from InSAR and GPS data. Geophys. Res. Lett. 44, 6778–6787. https://doi.org/10.1002/2017GL073580.

D'Agostino, N., 2014. Complete seismic release of tectonic strain and earthquake recurrence in the Apennines (Italy). Geophys. Res. Lett. 41 (4), 1155–1162. https://doi.org/10.1002/2014GL059230.

D'Agostino, N., Silverii, F., Amoroso, O., Convertito, V., Fiorillo, F., Ventafridda, G., Zollo, A., submitted for publication. Crustal deformation and seismicity modulated by groundwater recharge of karst aquifers. Geophys. Res. Lett.

De Vita, P., Allocca, V., Manna, F., Fabbrocino, S., 2012. Coupled decadal variability of the North Atlantic Oscillation, regional rainfall and karst spring discharges in the Campania region (southern Italy). Hydrol. Earth Syst. Sci. 16, 1389–1399. https://doi.org/10.5194/hess-16-1389-2012.

Devoti, R., Riguzzi, F., Cinti, F.R., Ventura, G., 2018. Long-term strain oscillations related to the hydrological interaction between aquifers in intra-mountain basins: a case study from Apennines chain (Italy). Earth Planet. Sci. Lett. 501. https://doi.org/10.1016/j.epsl.2018.08.014.

Di Matteo, L., Valigi, D., Cambi, C., 2013. Climatic characterization and response of water resources to climate change in limestone areas: some considerations on the importance of geological setting. J. Hydrol. Eng. 18, 773–779. https://doi.org/10.1061/(ASCE)HE.1943-5584.0000671.

Feigl, K.L., Thatcher, W., 2006. Geodetic observations of post-seismic transients in the context of the earthquake deformation cycle. C. R. Géosci. 338, 14–15. https://doi.org/10.1016/j.crte.2006.06.006.

Fiorillo, F., 2011. Tank-reservoir drainage as a simulation of the recession limb of karst spring hydrographs. Hydrogeol. J. 19, 1009–1019. https://doi.org/10.1007/s10040-011-0737-y.

Fiorillo, F., Doglioni, A., 2010. The relation between karst spring discharge and rainfall by cross-correlation analysis (Campania, Southern Italy). Hydrogeol. J. 18 (8), 1881–1895. https://doi.org/10.1007/s10040-010-0666-1.

Fiorillo, F., Pagnozzi, M., Ventafridda, G., 2015a. A model to simulate recharge processes of Karst Massifs. Hydrol. Process. 29, 2301–2314. https://doi.org/10.1002/hyp.10353.

Fiorillo, F., Petitta, M., Preziosi, E., Rusi, S., Esposito, S., Tallini, M., 2015b. Long-term trend and fluctuations of karst spring discharge in a Mediterranean area (Central-Southern Italy). Environ. Earth Sci. 74, 153–172. https://doi.org/10.1007/s12665-014-3946-6.

Gualandi, A., Serpelloni, E., Belardinelli, M.E., 2014. Space–time evolution of crustal deformation related to the $M_w$ 6.3, 2009 L'Aquila earthquake (central Italy) from principal component analysis inversion of GPS position time-series. Geophys. J. Int. 197, 174–191. https://doi.org/10.1093/gji/ggt522.

Johnson, C.W., Fu, Y., Bürgmann, R., 2017. Seasonal water storage, stress modulation, and California seismicity. Science 356 (6343), 1161–1164. https://doi.org/10.1126/science.aak9547.

King, N.E., et al., 2007. Space geodetic observation of expansion of the San Gabriel Valley, California, aquifer system, during heavy rainfall in winter 2004–2005. J. Geophys. Res. 112, B03409. https://doi.org/10.1029/2006JB004448.

LeGrand, H.E., Stringfield, V.T., 1971. Water levels in carbonate rock terranes. Ground Water 9, 4–10. https://doi.org/10.1111/j.1745-6584.1971.tb03544.x.

Métois, M., D'Agostino, N., Avallone, A., Chamot-Rooke, N., Rabaute, A., Duni, L., Kuka, N., Koci, R., Georgiev, I., 2015. Insights on continental collisional processes from GPS data: dynamics of the Peri-Adriatic belts. J. Geophys. Res., Solid Earth 120, 8701–8719. https://doi.org/10.1002/2015JB012023.

Milanović, P., 2014. Hydraulic properties of karst groundwater and its impacts on large structures. In: Mudry, J., Zwahlen, F., Bertrand, C., LaMoreaux, J.W. (Eds.), H2Karst Research in Limestone Hydrogeology. Springer International Publishing, Cham, pp. 19–48.

Moro, M., et al., 2017. New insights into earthquake precursors from InSAR. Sci. Rep. 7, 12035. https://doi.org/10.1038/s41598-017-12058-3.

Petitta, M., Caschetto, M., Galassi, D.M.P., Aravena, R., 2015. Dual-flow in karst aquifers toward a steady discharge spring (Presciano, Central Italy): influences on a subsurface groundwater dependent ecosystem and on changes related to post-earthquake hydrodynamics. Environ. Earth Sci. 73, 2609. https://doi.org/10.1007/s12665-014-3440-1.

Petitta, et al., 2018. Water-table and discharge changes associated with the 2016–2017 seismic sequence in central Italy: hydrogeological data and a conceptual model for fractured carbonate aquifers. Hydrogeol. J. 1 (18). https://doi.org/10.1007/s10040-017-1717-7.

Romano, E., Preziosi, E., 2013. Precipitation pattern analysis in the Tiber River basin (Central Italy) using standardized indices. Int. J. Climatol. 33, 1781–1792. https://doi.org/10.1002/joc.3549.

Romano, E., Del Bon, A., Petrangeli, B., Preziosi, E., 2013. Generating synthetic time series of springs discharge in relation to standardized precipitation indices. Case study in Central Italy. J. Hydrol. 507, 86–99. https://doi.org/10.1016/j.jhydrol.2013.10.020.

Rovida, A., Camassi, R., Gasperini, P., Stucchi, M. (Eds.), 2015. CPTI15, The 2015 Version of the Parametric Catalogue of Italian Earthquakes. INGV, Milano, Bologna. http://emidius.mi.ingv.it/CPTI15.

Schurch, M., Vuataz, F.D., 2000. Groundwater components in the alluvial aquifer of the alpine Rhone River valley, Bois de Finges area, Wallis Canton, Switzerland. Hydrogeol. J. 8, 549–563. https://doi.org/10.1007/s100400000094.

Serpelloni, E., Pintori, F., Gualandi, A., Scoccimarro, E., Cavaliere, A., Anderlini, L., Belardinelli, M.E., Todesco, M., 2018. Hydrologically-induced karst deformation: insights from GPS measurements in the Adria–Eurasia plate boundary zone. J. Geophys. Res., Solid Earth 123. https://doi.org/10.1002/2017JB015252.

Silverii, F., 2016. Study of the Transient Deformation of Central and Southern Apennines from GPS Observations. Dissertation thesis, Alma Mater Studiorum Università di Bologna. Dottorato di ricerca in Geofisica, 28 Ciclo.

Silverii, F., D'Agostino, N., Métois, M., Fiorillo, F., Ventafridda, G., 2016. Transient deformation of karst aquifers due to seasonal and multiyear groundwater variations observed by GPS in southern Apennines (Italy). J. Geophys. Res., Solid Earth 121, 8315–8337. https://doi.org/10.1002/2016JB013361.

Tsai, V.C., 2011. A model for seasonal changes in GPS positions and seismic wave speeds due to thermoelastic and hydrologic variations. J. Geophys. Res. 116, B04404. https://doi.org/10.1029/2010JB008156.

Wahr, J., Khan, S.A., van Dam, T., Liu, L., van Angelen, J.H., van den Broeke, M.R., Meertens, C.M., 2013. The use of GPS horizontals for loading studies, with applications to Northern California and southeast Greenland. J. Geophys. Res., Solid Earth 118, 1795–1806. https://doi.org/10.1002/jgrb.50104.

Wang, C.Y., Manga, M., 2010. Earthquakes and Water. Springer-Verlag, Berlin. 218 pp.

Wessel, P., Smith, W.H.F., Scharroo, R., Luis, J.F., Wobbe, F., 2013. Generic mapping tools: improved version released. Eos Trans. AGU 94 (45), 409–410. https://doi.org/10.1002/2013EO450001.